DOI: 10.26599/FSHW.2025.9250647

Contents lists available at SciOpen

Food Science and Human Wellness

journal homepage: https://www.sciopen.com/journal/2097-0765

China Food Publishing Co.

Docosahexaenoic acid-acylated astaxanthin esters alleviate cisplatin- induced acute kidney injury by modulating the ferroptosis-related GPX4/xCT signaling pathway and reducing oxidative stress

Youyan Wang[a], Lipin Chen[a,b,c], Haohao Shi[a,b,c*], Jierui Zhao[a], Penglin Xiang[a], Zhongyuan Liu[a,b], Guanghua Xia[a,b], Yuming Wang[c]

[a] *School of Food Science and Engineering, Hainan University, Haikou 570228, China*

[b] *Key Laboratory of Food Nutrition and Functional Food of Hainan Province, Haikou 570228, China*

[c] *SKL of Marine Food Processing & Safety Control, College of Food Science and Engineering, Ocean University of China, No.1299 Sansha Road, Qingdao 266404, P.R. China*

ABSTRACT: Acute kidney injury (AKI) can be caused by various factors, such as renal ischemia and hypoxia, drug toxicity, and malnutrition, leading to a rapid decline in renal function, abnormal nitrogen metabolism, or reduced urine output. Previous studies have reported that astaxanthin (AST) has a protective effect on the kidneys, and the main form of acylated AST (AST-DHAs) widely found in seafood is docosahexaenoic acid-acylated monoester (AST-DHA) and diester (AST-2DHA). In this study, we successfully prepared AST-DHAs through enzymatic/chemical methods and constructed a mouse model of cisplatin-induced acute kidney injury (AKI) to explore the impact of AST-DHAs on AKI. The experimental results are interesting: compared with the model group, AST-DHA treatment showed strong efficacy. It not only significantly enhanced the renal function of mice and significantly reduced urea nitrogen and creatinine levels but also significantly reduced pathological damage and oxidative stress. Moreover, AST-DHA treatment significantly upregulated the expression of the ferroptosis core protein, glutathione peroxidase 4, and the cystine/glutamate transporter. Further metabolomic analysis revealed that AST-DHAs can regulate the related changes in mice caused by AKI and effectively improve the AKI status of mice by inhibiting ferroptosis. These results strongly indicate that AST-DHAs are likely potential therapeutic adjuvants for alleviating AKI, providing a new direction and hope for the treatment of acute kidney injury.

1. Introduction

Acute kidney injury (AKI) is characterized by a rapid decline in kidney function, metabolic waste retention, and imbalances in water, electrolytes, and acid-base homeostasis. The global incidence of AKI is 21.6% and 33.7% in children.[1] The International Society of Nephrology has reported that patients with AKI are at an increased risk of developing chronic kidney disease, uremia, cardiovascular events, and mortality.[2] AKI poses significant medical and financial burdens affecting patients, families, and society globally.[3] The mechanisms underlying AKI are multifaceted and include renal ischemia, vasoconstriction, reactive oxygen

***Corresponding author**
shihaohao@hainanu.edu.cn

Received 19 September 2024
Received in revised from 7 January 2025
Accepted 3 April 2025

species (ROS), tubular toxicity, obstructive injury, inflammation, edema, and reduced glomerular filtration capacity.[4] Various factors such as drug use (e.g., cisplatin and gentamicin), cardiac and surgical procedures, shock, and end-stage illnesses can trigger AKI.[5] Therefore, AKI has emerged as a significant challenge hindering the progress of various clinical medical fields, such as surgery, transplantation, cardiovascular medicine, interventional radiology, and oncology.[6] Currently, AKI treatment can only relieve the symptoms of kidney disease and does not provide a complete cure. Therefore, finding a suitable method to reduce renal toxicity remains an urgent and unfinished mission. The intricacies of renal toxicity are multifaceted; thus, the pursuit of natural, bioactive compounds that demonstrate significant renoprotective properties has captivated the interest of scientists.[7]

Astaxanthin is a red lipid-soluble keto-carotenoid with various biological activities, such as anticancer, anti-inflammatory, immunostimulatory, and extremely strong antioxidant properties.[8] Astaxanthin is widely distributed in nature, and its beta-ionone at C3/C30 is unstable and easily oxidized.[9] Therefore, the terminal hydroxyl group is often esterified by fatty acids, and according to the number of fatty acids it combines with, it can be divided into astaxanthin monoesters (AST-MEs) and astaxanthin diesters (AST-DEs).[10] Compared to free astaxanthin, astaxanthin esters, as derivatives of astaxanthin, exhibit superior bioavailability, thermal stability, light stability, and antioxidant capacity.[11] For example, Kobayashi et al. conducted a comparative study on the singlet oxygen quenching activity of astaxanthin, astaxanthin single ester and double ester, β-carotene, and carotene.[12] A photooxidation experiment using linoleic acid demonstrated that the astaxanthin ester exhibited the highest singlet oxygen quenching ability among all the compounds tested. Additionally, Rao investigated the antioxidant activity of the astaxanthin ester in vivo by administering it to mice with carbon tetrachloride-induced liver injury.[13] These results revealed the significant liver protection and antioxidant effects of astaxanthin ester. Furthermore, Kamath et al. examined the impact of total carotenoids and astaxanthin esters from *Rhodococcus vulvae* on gastric ulcers in rats and revealed that *R. vulvae*-derived astaxanthin esters exerted gastroprotective effects through an antioxidant mechanism while preventing and protecting against gastric ulcers.[14] In addition, studies have shown that astaxanthin esters have distinct effects on medical treatment, cosmetic beauty, and functional foods.[15] These effects include treating inflammatory bowel disease, enhancing antioxidant capacity, preventing Parkinson's disease (PD), improving insulin resistance, increasing immunity, increasing heat stability, facilitating digestion and absorption, and regulating the intestinal microbiota, among other biological activities. Astaxanthin is notably found in a variety of marine organisms, existing not only as unesterified AST but also as fatty acid-acylated AST esters.[16] Specifically, docosahexaenoic acid-acylated astaxanthin esters (AST-DHAs) represent a chemical composite of AST combined with DHA. Depending on the number of fatty acids attached, AST-DHAs can be categorized into astaxanthin monoesters acylated with docosahexaenoic acid (AST-DHA) and astaxanthin diesters acylated with docosahexaenoic acid (AST-2DHA). In a study by Wang et al., Parkinson’s disease (PD) was induced in mice using 1-methyl-4-phenyl-1,2,3,6-tetrahydropyridine (MPTP) to evaluate the impact of AST-DHAs on the disease.[17] The findings revealed that AST-DHA

significantly reduced the incidence of MPTP-induced PD in mice, with efficacy surpassing that of both AST alone and the combination of AST with DHA. The most pronounced inhibitory effect was observed regarding apoptosis in dopaminergic neurons through the mitochondria-mediated c-Jun N-terminal kinase (JNK) and P38 mitogen-activated protein kinase (MAPK) pathways. Moreover, AST-DHAs facilitated the proliferation of cyclooxygenase-2 (COX-2)-producing cells within a concentration range of 10 to 40 μg/mL.Furthermore, they exhibited the ability to mitigate oxidative cell damage by lowering levels of malondialdehyde and lactate dehydrogenase while enhancing the release of superoxide dismutase, which acts to control ROS levels within the cells.[18] Additionally, AST-DHAs can neutralize or interrupt free radical chain reactions, restoring immune defense mechanisms and boosting overall immunity.[19]

Although AST-DHAs have various biological activities, the effects of astaxanthin in a cisplatin (CP)-induced AKI model have not been reported. However, whether AST-DHAs exert preventive and therapeutic effects against kidney injury remains unknown. In this study, an acute kidney injury model induced by CP was established in mice to investigate the protective effects of AST-DHAs on acute kidney injury and the underlying mechanism. The analysis included the evaluation of body weight, kidney index, and renal function indices, as well as histopathological examination of renal tissue sections. Furthermore, we conducted an immunofluorescence examination of glutathione peroxidase 4 (GPX4) and cystine/glutamate transporter (xCT), alongside non-targeted metabolomic profiling and the assessment of oxidative stress markers to clarify the mechanisms by which AST-DHAs influence acute kidney injury (AKI) in mice. This research lays a foundational theoretical and scientific framework for creating functional foods, implementing nutritional strategies, and developing innovative and effective therapeutic agents aimed at addressing CP-induced AKI.

2. Materials and methods

2.1 Experimental materials and reagents

Docosahexaenoic acid-acylated astaxanthin esters were produced using enzymatic and chemical methods outlined in a prior investigation.[20] The CP (product lot number: MKCS6808) was sourced from Merck Sigma Aldrich (Shanghai) Trading Co., Ltd. located in Shanghai, China. Determination kits for blood urea nitrogen (BUN), uric acid (UA), creatinine (CRE), malondialdehyde (MDA), superoxide dismutase (SOD), glutathione (GSH), glutathione peroxidase (GSH-Px), and bicinchoninic acid (BCA) protein concentration were procured from the Nanjing Jiancheng Institute of Biological Engineering in Nanjing, China. Antibodies for GPX4 and xCT were obtained from Wuhan Sevier Biotechnology Co., Ltd. in Wuhan, China. All other chemicals and reagents utilized were of analytical caliber.

2.2 Animal experiments

A total of 80 six-week-old male BALB/c mice were acquired from Hunan Lake Jingda Technology Co., Ltd. (Hunan, China). The standard diet was sourced from the Guangdong Medical Laboratory Animal Center (Guangdong, China), and the animal housing environment was kept at a temperature of 25 ± 2 °C

with humidity levels of 55 ± 5%, in accordance with specific pathogen free sanitary guidelines. The mice experienced a daily light-dark cycle of 12 hours and had unlimited access to feed and autoclaved water. Additionally, bedding was refreshed every three days, along with the provision of new drinking water and food. All experimental procedures adhered to China's Regulations on the Administration of Experimental Animals and received approval from the Ethics Committee of Hainan University, China (HNUAUCC-2023-00137).

After a week of adaptive feeding, a total of 80 mice were randomly assigned to eight different groups (n = 10): normal control (C), model (M), AST, DHA, AST-DHA monoester (DHA-acylated AST), AST-2DHA diester group (DHA-acylated AST), a combination of equal amounts of non-esterified AST and DHA (AST+DHA), and non-esterified AST with double the amount of DHA (AST+2DHA). Each group of mice received daily administration of their respective samples. The dosage for the AST group was set at 60 mg/kg/day, while the DHA group received a dosage of 33 mg/kg/day. Treatment was carried out through oral gavage once daily for a period of 12 days. Prior to treatment, the mice were pre-exposed to various substances for 10 days, followed by intraperitoneal injection of a CP solution at a dose of 20 mg/kg. After 12 days, the mice were euthanized, and blood along with tissue samples were gathered for analysis. (The experimental process is illustrated in Fig. S1.)

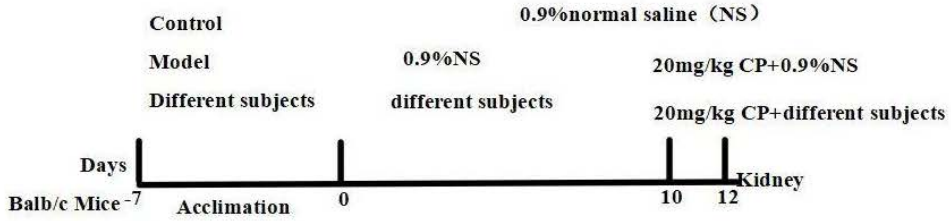

Figure S1. Establishment of cisplatin-induced acute kidney injury model and treatment flow chart of the differently treated mice.

2.3 Blood and tissue sample collection

Prior to the collection of tissue samples, the daily weight of each group of mice was recorded, and the mean weight for every group was determined. The kidneys were then weighed, using the following formula: organ weight index = [organ wet weight (g)/body weight (g)] × 100.

Following the 12-day treatment period, all mice were subjected to a 12-hour fasting, although they were permitted to drink autoclaved water. Subsequently, the mice were euthanized, and samples of blood and tissue were gathered. Blood samples were obtained by excising the eyeballs of the mice with tweezers. These samples remained at room temperature for 30 minutes before being centrifuged at 4 °C at a speed of 3000 rpm for 15 minutes to facilitate serum separation. The collected serum was then stored at –80 °C for future analyses. Kidneys were promptly extracted and rinsed with pre-cooled saline to eliminate any blood. After being blotted on filter paper, the weight was measured using a precision electronic balance; the left kidney was immersed in a prepared formalin solution for later use, while the right kidney was retained in a freezer set at −80 °C until required.

2.4 Biochemical indicator determination

Serum concentrations of creatinine (Cr), blood urea nitrogen (BUN), and uric acid (UA) were assessed employing commercial assay kits as per the guidelines provided by the manufacturer. Following the weighing process, kidney samples underwent homogenization in nine volumes of 0.9% normal saline, after which the homogenates were centrifuged at 3000 rpm for a duration of 10 minutes to collect the supernatant. Protein levels were evaluated utilizing a BCA assay kit. The activities of malondialdehyde (MDA), superoxide dismutase (SOD), glutathione (GSH), and glutathione peroxidase (GSH-Px) were measured in 10% tissue homogenates in accordance with the manufacturer's instructions.

2.5 Histological analysis

For histological analysis, we fixed a portion of the kidney to 4% formaldehyde, rinsed with water for 10 min, dehydrated with alcohol (75%, 85%, 95%, and 100%) in the usual sequence, and treated with xylene to render it transparent. The samples were embedded in paraffin wax. The microscopic holes used for sample cutting were thickened to 5μm. Histological staining with Hematoxylin-eosin (H&E) staining was used to evaluate the degree of kidney injury, including tubular necrosis, inflammatory infiltration, interstitial edema, tubular atrophy or dilation, etc. The paraffin-embedded kidney sections were subjected to Masson's staining to evaluate the degree of renal fibrosis. Under a microscope, the collagen fibers are blue, the muscle fiber cytoplasm is red, and the nuclei are –brown.[21]

2.6 Renal fatty acid composition

Mouse kidneys were removed from a methyl ester test tube, methyl ester reagent (methanol: hydrochloric acid = 5:1, v/v) was added, and the tube was filled with nitrogen, sealed, and fully swirled. The tube was bathed in water at 90 °C for 3 h, during which time the methyl ester tube was removed every 30 min and swirled for 30 s. After the water bath was completed, the test tube containing the methyl ester was taken out and allowed to cool to room temperature. Following this, n-hexane was introduced, and after stratification, the upper layer of n-hexane was carefully separated. Nitrogen gas was then used to dry the sample, gas chromatography was employed to determine the concentration, and the alterations in fatty acids in mouse kidneys were examined.[22]

2.7 Renal immunohistochemistry-DAB-enhanced Prussian blue staining

The histochemical determination of iron storage in kidney tissue was carried out using Perls' Prussian blue, which was enhanced with diaminobenzidine (DAB)[23]. Following the established protocol, the tissue sections were immersed in a Prussian blue solution (Servicebio, Wuhan, China) and allowed to incubate at room temperature for 30 minutes. Subsequently, DAB chromogenic solution (Servicebio, Wuhan, China) was incorporated to amplify the staining process, also at room temperature. After the staining procedure, all sections underwent rinsing, dehydration, and were then cover slipped before being digitized using a light microscope (Nikon, Japan).

2.8 Kidney immunofluorescence

In accordance with the methods of Zheng et al.,[24] immunofluorescence staining was performed on mouse kidneys. The quantitative assessment of glutathione peroxidase (GPX4) and cystine/glutamate transporter (xCT), essential elements in ferroptosis, was performed in the kidneys using fluorescence labeling. The procedure included antigen retrieval, incubation with antibodies, DAPI solution staining for the cell nucleus, and subsequent visualization through fluorescence emission for image capture.

2.9 LC–MS untargeted metabolomics

Metabolomics employing LC–MS untargeted techniques was executed on mouse kidneys as outlined by Quancheng Cheng et al.[25]. A total of 50 mg mouse kidney samples was placed into a 2 mL centrifuge tube, to which a 6 mm grinding bead was added. For the extraction of metabolites, 400 μL of an extraction solution (methanol:water in a 4:1 volumetric ratio) containing an internal standard (L-2-chlorophenylalanine) at a concentration of 0.02 mg/mL was utilized. The samples were subjected to grinding using a Wonbio-96c frozen tissue grinder (Shanghai Wanbo Biotechnology Co., Ltd.) for a duration of 6 minutes (–10 °C, 50 Hz). Subsequently, low-temperature ultrasonic extraction was performed for 30 minutes (5 °C, 40 kHz). Afterward, the samples were stored at –20 °C for 30 minutes and then centrifuged at 13000 × g at 4 °C for 15 minutes. Finally, the resulting supernatant was collected and transferred into an injection vial for subsequent LC–MS/MS analysis.[26]

Analysis of the samples using LC–MS/MS was performed on a Thermo UHPLC-Q Exactive HF-X system that featured an ACQUITY HSS T3 column (100 mm × 2.1 mm i.d., 1.8 μm; Waters, USA) at Majorbio Bio-Pharm Technology Co., Ltd. located in Shanghai, China. For the mobile phase, a mixture of 0.1% formic acid in water and acetonitrile (95:5, v/v) was used as solvent A, while solvent B consisted of 0.1% formic acid in a blend of acetonitrile, isopropanol, and water (47.5:47.5, v/v). The column temperature was maintained at 45 °C, and the flow rate was set at 0.40 mL/min, with an injection volume of 10 μL.

For the analysis of untargeted metabolomics, the raw LC-MS data underwent preprocessing with Progenesis QI software (Waters Corporation, Milford, USA), resulting in a three-dimensional data matrix that was exported in CSV format. The data matrix, acquired through database searching, was then uploaded to the Majorbio Cloud platform (https://cloud.majorbio.com) for further analysis. Subsequently, principal component analysis, orthogonal partial least squares discriminant analysis (OPLS-DA), and a 7-cycle interactive validation were conducted using the R package “ropls” (version 1.6.2) to assess the model's stability. Metabolites exceeding a variable importance in projection (VIP) of 1 and a p-value of less than 0.05 were identified as significantly different based on VIP values from the OPLS-DA model and p-values obtained from Student’s t-test. The differentially abundant metabolites between the two groups were aligned with their biochemical pathways through metabolic enrichment and pathway analyses, utilizing the Kyoto Encyclopedia of Genes and Genomes (KEGG) database (http://www.genome.jp/kegg/).

2.10 Statistical analysis

Each experiment was conducted independently in triplicate, and the results are presented as the mean ± standard error of the mean (SEM). Statistical analysis of all data was performed using one-way analysis of

variance (ANOVA), followed by Tukey's multiple comparison test. A p-value of less than 0.05 was deemed to represent statistical significance.

3. Results

3.1 Effects of AST-DHAs on kidney and liver indices

As shown in Figure 1B and D, the kidney and liver weights were significantly greater in group M than in group C ($p < 0.01$), but these effects were significantly reversed after treatment with AST-DHA and AST-2DHA ($p < 0.05$). Organ index is a commonly used indicator in pharmacological/toxicology experiments, and the ratio of kidney weight to body weight is relatively constant under normal physiological conditions.[27] After the body of an animal is damaged, the weight and coefficient of the organs change. Consequently, the visceral ratio serves as a clear indicator for assessing the extent of bodily injuries. As illustrated in Figures 1A and C, the indices for the kidneys and liver in the CP-injected cohort were markedly elevated compared to the control group ($p < 0.05$). Moreover, when contrasted with the M group, the kidney and liver indices in both the AST-DHA and AST-2DHA groups were reduced, with the AST-2DHA group showing a significantly lower value ($p < 0.05$). These results indicate that CP-induced acute kidney injury in mice has been successfully established and that the kidney and liver indices of mice are significantly increased, resulting in hyperemia, edema, hyperplasia, and hypertrophy of the liver and kidney.[28] However, AST-DHAs significantly reduced the kidney and liver indices and body weight of mice injected with CP, suggesting that AST-DHAs have a protective effect in mice with AKI.

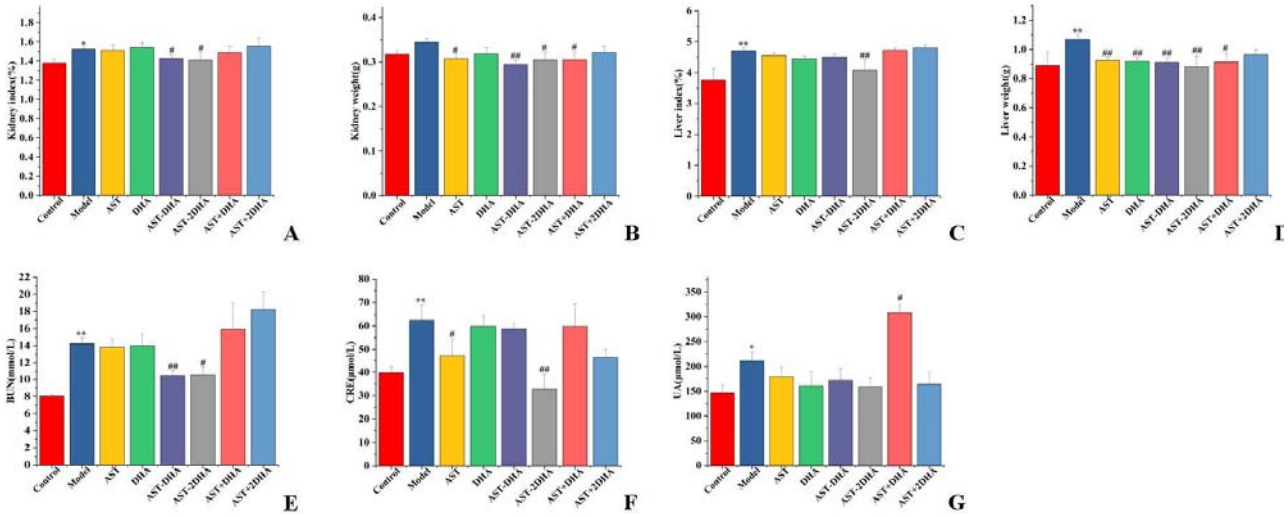

Figure 1. The impact of various samples on (A) kidney index, (B) kidney weight, (C) liver index, (D) liver weight, (E) serum urea nitrogen (BUN), (F) creatinine (CRE), and (G) uric acid (UA) in mice was assessed. Data are presented as mean ± S.E.M. for a total of 8 mice. ** Indicates a significant difference when compared to the control group ($p < 0.01$); ## Indicates a significant difference relative to the model group ($p < 0.01$).

3.2 Effects of AST-DHAs on Renal Function Biomarkers

BUN, CRE, and UA levels are often used as indicators of kidney function.[29] Figure 1E–G illustrates that the levels of BUN ($p < 0.01$), CRE ($p < 0.01$), and UA ($p < 0.05$) in group M were notably elevated compared to those in group C, suggesting a successful establishment of the CP-induced AKI model. In contrast to the M group, the BUN levels in the AST-DHA and AST-2DHA groups were significantly reduced ($p < 0.05$), while

the CRE level in the AST-2DHA group also demonstrated a significant decrease ($p < 0.01$). There was no significant difference in the expression level of UA between the AST-DHA, AST-2DHA, and M groups ($p > 0.05$); however, UA decreased to a certain extent. These results indicated that AST-DHAs have beneficial interventional effects on AKI. Thus, AST-DHAs may serve as effective adjuvants for the prevention and treatment of AKI.

3.3 Effects of AST-DHAs on histopathology

As shown in Figure 2A, the cellular structure of the kidney tissue in the normal group was normal; the tubular cells were neatly arranged, the tubules and glomeruli were normally shaped, and the boundaries between cells were clear. The renal tissue structure of the model group was disrupted, and many large vacuoles were observed with disordered structural arrangements and degenerative changes in the proximal tubules, such as loss of brush edges and pale cytoplasmic staining. Renal tubular epithelial cells exhibited degeneration and necrosis, alongside notable alterations in glomerular structure and infiltration by inflammatory cells. Upon administration of AST-DHAs, the extent of renal tissue damage was markedly more severe compared to the model group; in particular, the organization of renal tubular cells appeared more orderly, leading to a decrease in the necrosis of these cells, the occurrence of expansion, the quantity of vacuoles, and the infiltration by inflammatory cells. Compared to the other groups, the treatment groups presented greater therapeutic effects and greater reductions in kidney damage. Comparing the AST-DHA and AST-2DHA groups, the diester group exhibited more significant reductions in damage, as evidenced by the more regular arrangement of tubular cells and fewer vacuoles.

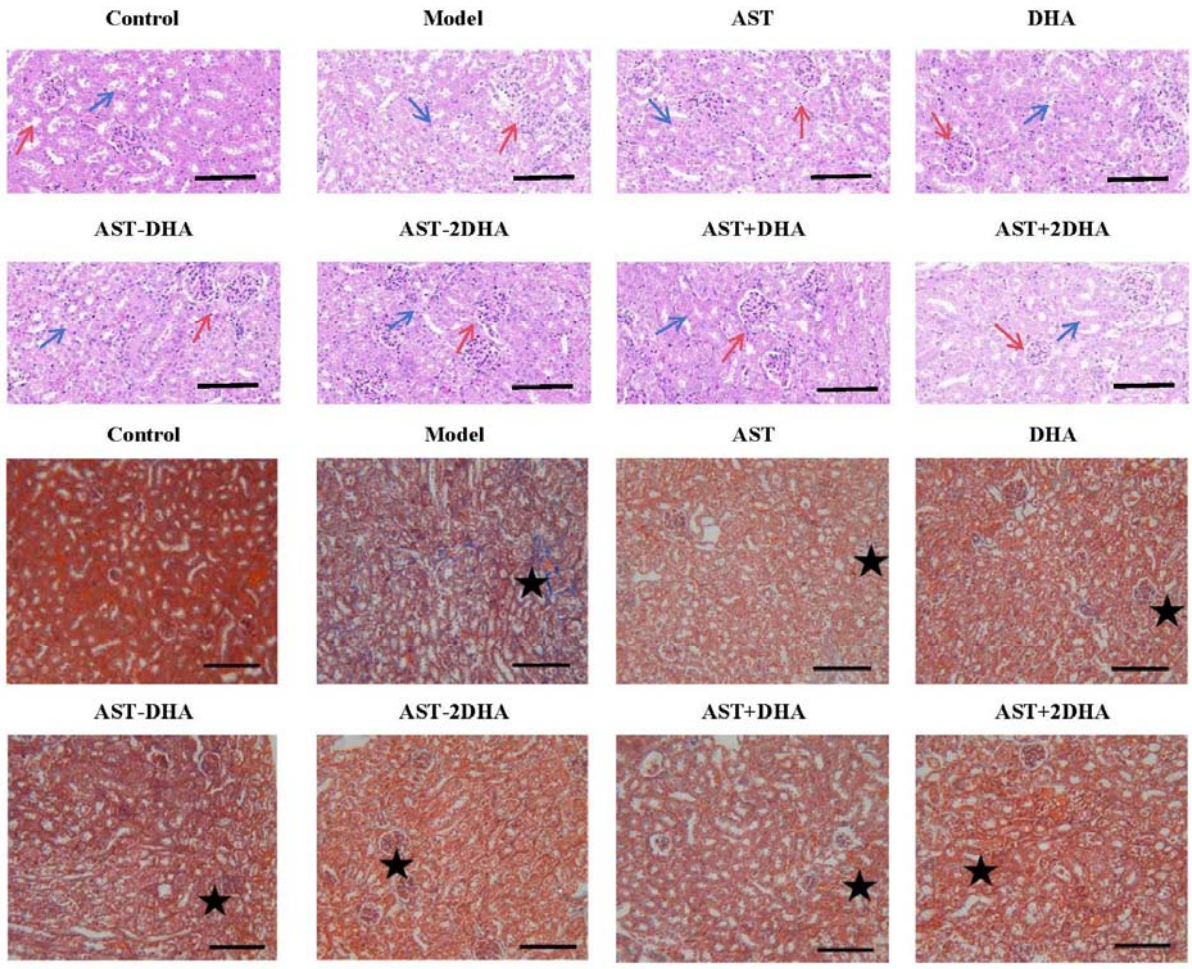

Figure 2. Histopathological results of acute kidney injury as assessed by (A) H&E staining and (B) Masson's staining of kidney tissues (200× magnification, n=10). Green arrows indicate glomerular necrosis, blue arrows indicate vacuolization, and the stars indicate renal fibrosis. Scale bar = 50 μm; 200× magnification.

Masson's staining was employed to examine the pathological tissue and collagen architecture by targeting collagen and muscle fibers.[30] Consequently, this staining technique was utilized to assess the extent of renal fibrosis in the mice, and the impact of AST-DHAs on CP-induced AKI in the mice was evaluated. As illustrated in Figure 2B, the findings indicated that the myocardial fibers in group C were orderly arranged, and the level of fibrosis was minimal. The glomeruli had a complete and clear structure, with an ordered arrangement, and no signs of fibrosis. Compared with group C, the myocardial fiber arrangement in group M was disrupted, the degree of myocardial fibrosis was greater, glomerular atrophy was observed, surrounding tissue fibrosis and arrangement disorders were observed, and the nucleus largely escaped. These results indicated that CP-induced renal fibrosis in mice was successfully established. The degree of myocardial fiber arrangement disorder and fibrosis in the AST-DHA group was greater than that in the M group. Compared to the M group, the glomerular morphology in the M group was full and complete, the degree of fibrosis was reduced, and the degree of fibrosis was clearly improved. Improvements in myocardial fiber arrangement and fibrosis severity in the AST-DHA group were greater than those in the AST-2DHA group, indicating that AST-2DHA improved these parameters to a greater extent. These results suggest that AST-DHA treatment improves renal fibrosis in mice with AKI.

3.4 Effects of AST-DHAs on renal fatty acids in mice

Saturated fatty acids are recognized as fundamental constituents of lipids. Typical examples of saturated fatty acids, such as palmitic acid (C16:0) and stearic acid (C18:0), play a crucial role in preserving the normal composition of fatty acids within the body. Polyunsaturated fatty acids (PUFAs) are essential nutrients for the human body. The fatty acid docosahexaenoic acid (C22:6) is a PUFA with various biological activities. These treatments include lipid-lowering, anti-inflammatory, antioxidant and immunomodulatory agents.[31] The concentrations of these fatty acids fluctuate in response to bodily damage. Consequently, the fatty acid profile of the mouse kidney underwent analysis using GC–MS. Figure 3 illustrates that the concentrations of C16:0, C18:0, and C22:6 were markedly reduced in group M compared to group C ($p < 0.05$), suggesting that CP injection led to a decrease in the fundamental fatty acid content among the mice, confirming the success of the model. Compared to the M group, the contents of C16:0, C18:0, and C22:6 in the AST-DHA treatment group increased to varying degrees, indicating that AST-DHAs can alleviate the decrease in saturated and unsaturated fatty acid content in mice with AKI. The levels of saturated and unsaturated fatty acids in the AST-2DHA group exceeded those observed in the AST-DHA group, suggesting that AST-2DHA alleviated this effect. Furthermore, these findings suggest that treatment with AST-DHA can counteract the reduction in saturated and unsaturated fatty acid levels in the kidneys of mice suffering from AKI, thereby supporting normal physiological function.

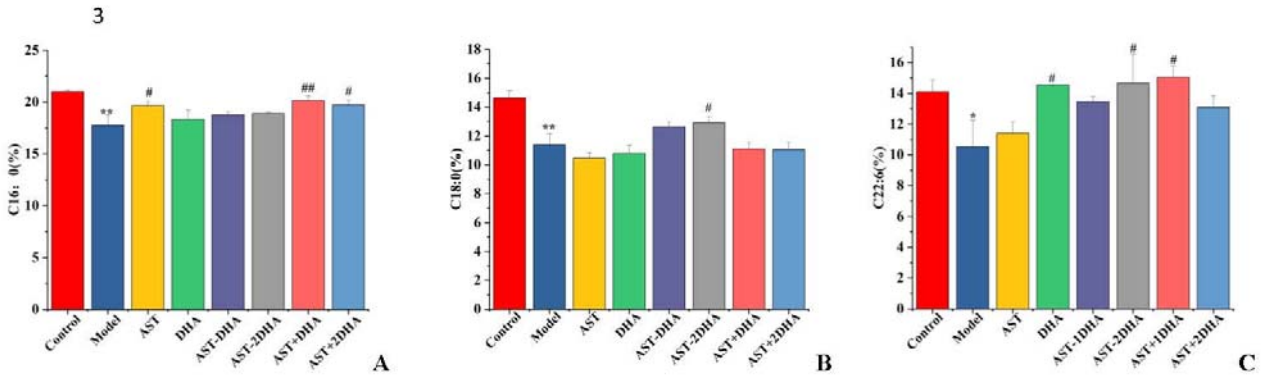

Figure 3. Influence of various samples on the alterations in fatty acid composition within mouse kidney tissue. (A) Palmitic acid (C16:0), (B) Stearic acid (C18:0), and (C) Docosahexaenoic acid (C22:6) were analyzed. The results are presented as mean ± S.E.M. from a sample of 8 mice. ** Indicates a significant difference when compared to the normal group ($p < 0.01$); ## Indicates a significant difference when compared to the model group ($p < 0.01$).

3.5 Effects of AST-DHAs on oxidative stress markers

The significant generation of reactive oxygen species (ROS) resulting from oxidative stress leads to oxidative harm to proteins, lipids, DNA, and various biological macromolecules, ultimately harming the human body. Compared to those in group C, the levels of SOD, GSH, and GSH-Px in the kidneys of group M were significantly lower ($p < 0.01$), whereas the MDA content was significantly higher ($p < 0.01$), suggesting that CP injection caused kidney damage. Following the pretreatment with AST-DHAs, the concentrations of SOD, GSH ($p < 0.01$), and GSH-Px observed in the kidneys of both the AST-DHA and AST-2DHA groups were markedly elevated compared to the M group, while the MDA levels were considerably reduced ($p <$

0.01), resembling the levels found in healthy mice (Figure 4A–D). The serum oxidative stress index showed a similar trend (Figure 4E–G). These results indicated that AST-DHAs can significantly reduce CP-induced oxidative damage and improve the antioxidant capacity of mice.

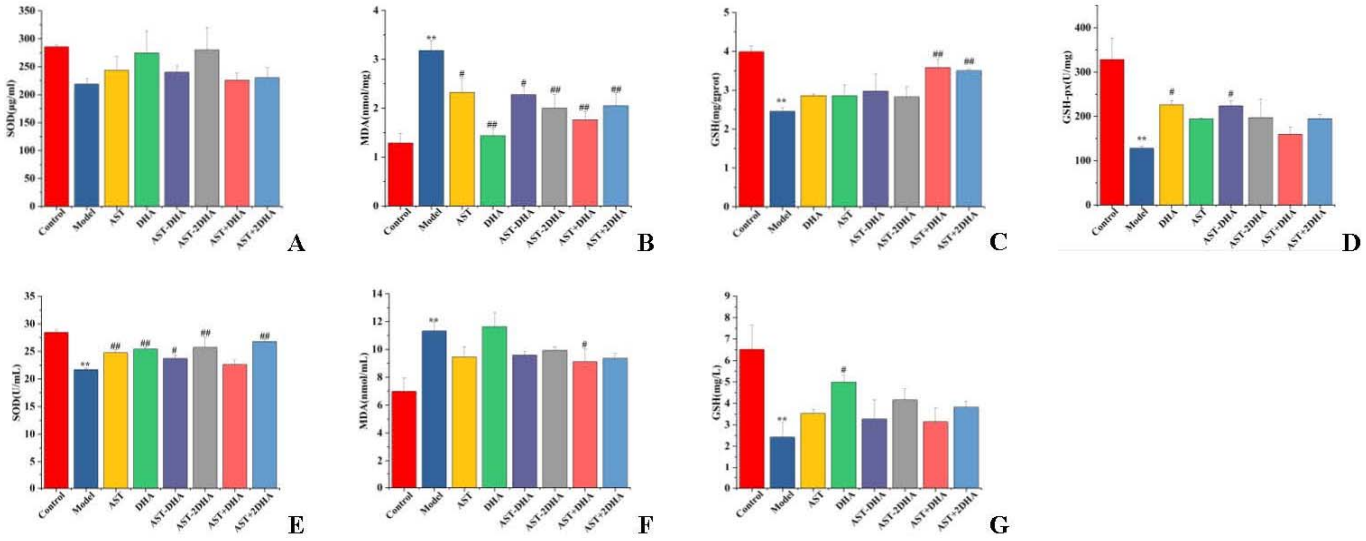

Figure 4. The influence of various samples on superoxide dismutase (SOD), malondialdehyde (MDA), glutathione (GSH), and glutathione peroxidase (GSH-Px) in kidney tissue from mice is illustrated in panels A to D; panels E to G highlight the impact of the different samples on SOD, MDA, and GSH levels in mouse serum. The results are presented as mean ± S.E.M. for a total of 8 mice. ** Indicates a significant difference when compared to the normal group ($p < 0.01$). ## Indicates a significant difference relative to the model group ($p < 0.01$).

3.6 Effects of AST-DHAs on renal iron accumulation in mice

Iron death refers to a form of programmed cell necrosis that occurs due to lipid peroxidation caused by iron ions and reactive oxygen species (ROS). This process is marked by an accumulation of iron and the occurrence of lipid peroxidation. Therefore, DAB-enhanced Prussian blue staining was used to perform immunohistochemical staining of kidney sections from mice in each group to observe the accumulation of iron ions in the kidneys. As shown in Figure 5, there was little iron deposition in group C but significant iron deposition in group M, indicating that cisplatin caused iron accumulation in the kidneys of mice, resulting in kidney damage. After AST-DHA treatment, iron deposition was alleviated. These results indicated that AST-DHAs can inhibit the accumulation of iron ions and exert protective effects against kidney injury in mice.

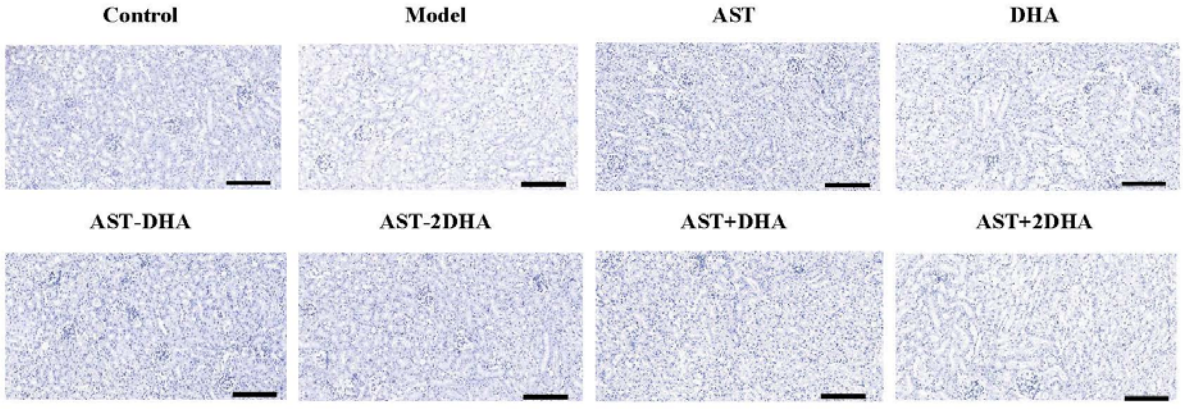

Figure 5. Effects of different samples on staining for iron accumulation in mouse kidney tissue using diaminobenzidine (DAB) enhanced Perls' staining (n=6). The iron-containing parts of the tissue are brown, and the nuclei are light blue. Scale bar = 50 μm; 200× magnification.

3.7 AST-DHAs upregulate GPX4/xCT signaling pathway in kidneys

Acute tubular necrosis is the primary pathological feature of AKI. Iron-dependent triggering, also known as iron cell death, is one of the main pathways involved in tubular cell necrosis. GPX4 and xCT are thought to play a crucial role in cell viability and serve as essential regulatory proteins in iron-induced cell death. GPX4 has the ability to break down small-molecule peroxides, along with certain lipid peroxides, thereby preventing lipid peroxidation. In exchange for intracellular glutamate, xCT can take up cystine and inhibit iron death. Therefore, in this study, we evaluated the localization of GPX4 and xCT using immunofluorescence staining with specific antibodies to identify GPX4- and xCT-positive cell types in mouse kidneys. As illustrated in Figure 6, the GPX4 and xCT expression levels in group M were found to be very low. Following pretreatment with AST-DHAs, there was a significant increase in the GPX4 expression in both tissues and cells compared to group M. Additionally, AST-DHAs contributed to a certain degree of upregulation in the expression of xCT. These findings imply that AST-DHAs have the potential to enhance the expression of GPX4 and xCT in the kidneys of mice after acute kidney injury induced by CP. In addition, immunofluorescence staining confirmed the colocalization of GPX4 and xCT, indicating that AST-DHA pretreatment increased the colocalization of GPX4–xCT.

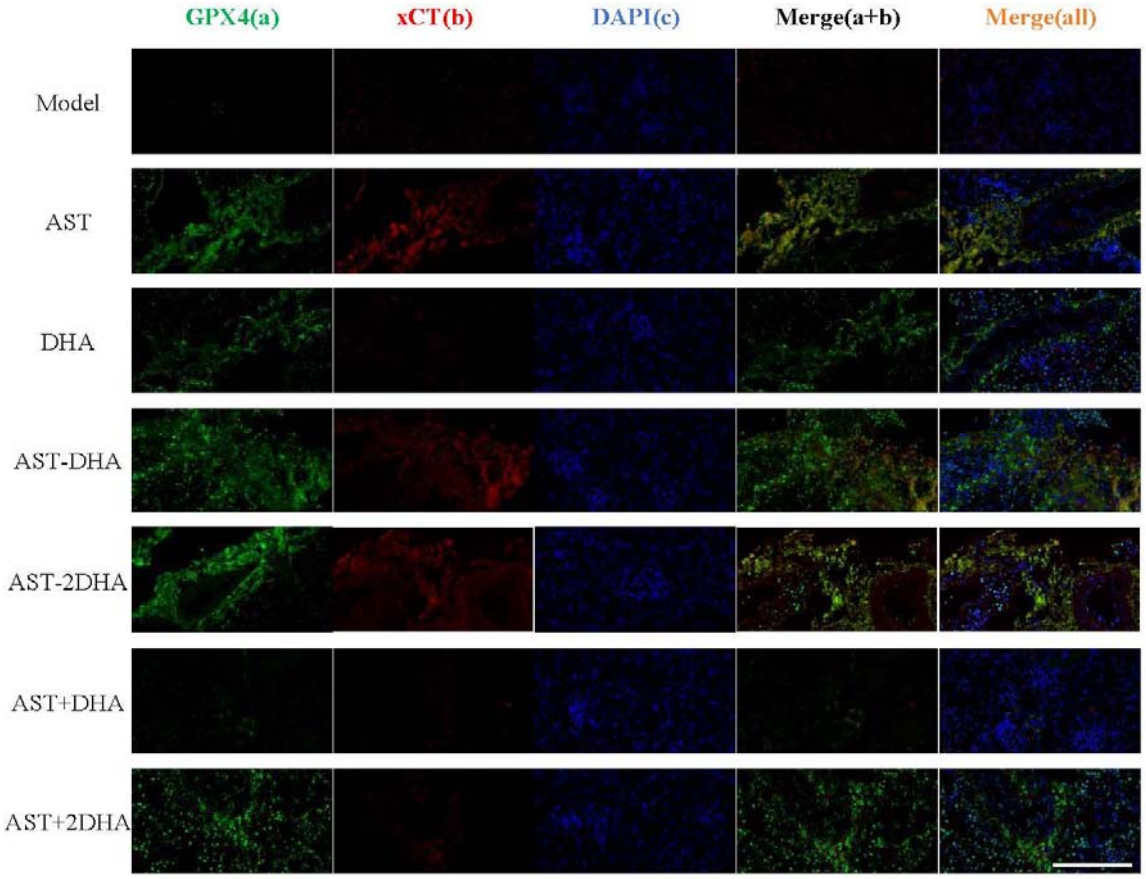

Figure 6. Impacts of various samples on glutathione peroxidase 4 (GPX4) and the cystine/glutamate transporter (xCT), which are indicators linked to ferroptotic cell death (n=6). The activation of ferroptosis localized during the progression of renal injury. Kidney tissue sections (5 μm thick), with a scale bar measuring 20 μm; magnification at 400×.

3.8 LC–MS untargeted metabolomics

These findings indicated that AST-DHA pretreatment alleviated CP-induced AKI in mice. To further analyze its therapeutic effect in mice AKI, kidney samples from mice in five of the groups (C, M, DHA, AST-DHA, and AST-2DHA) were collected for LC–MC untargeted metabolomics analysis. Changes in renal metabolites were observed to elucidate the mechanism by which AST-DHAs treat AKI.

3.9 Sample comparative analysis

The results of the metabolomic analysis were evaluated by creating a PLS-DA model, which employed partial least squares regression to formulate a regression model correlating metabolite expression levels with sample categories for the purpose of predicting sample classification. As illustrated in Figure 7A–C, the replicated samples from both the control and treatment groups displayed a close clustering in positive and negative ion modes, signifying the data's strong reproducibility. Compared with group C, group M showed obvious dispersion within and between the groups. These findings indicate that the CP-induced AKI model was successful. The AST-DHA and AST-2DHA groups were clustered within groups, clearly separated from the M group and similar to the C group. These findings indicated that pretreatment with AST-DHAs alleviated AKI in mice to some extent, the AST-DHA-treated group approaching that of the normal group. In addition, a total of 1,131 metabolites were identified by metabolomics. These metabolites included lipids and lipid-like molecules (379 metabolites, 33.51%), organic acids and their derivatives (215 metabolites, 19.01%), organic heterocyclic compounds (151 metabolites, 13.35%), organic oxidation products (113 metabolites, 9.99%), and phenylpropanoids and polyketides (74 metabolites, 6.54%) (Figure 7D). Analysis of the differentially abundant metabolites in group M revealed 344 different metabolites compared with those in group C, with 178 upregulated and 166 downregulated metabolites. Compared to the M group, the levels of 200 different metabolites in the AST-DHA group were 106 upregulated and 94 downregulated. Similarly, the levels of 171 metabolites in the AST-2DHA group differed from those in the M group, with 107 upregulated and 64 downregulated metabolites (Figure 7E–H). These findings suggest that the downregulation of differentially abundant metabolite expression was mitigated by AST-DHA treatment.

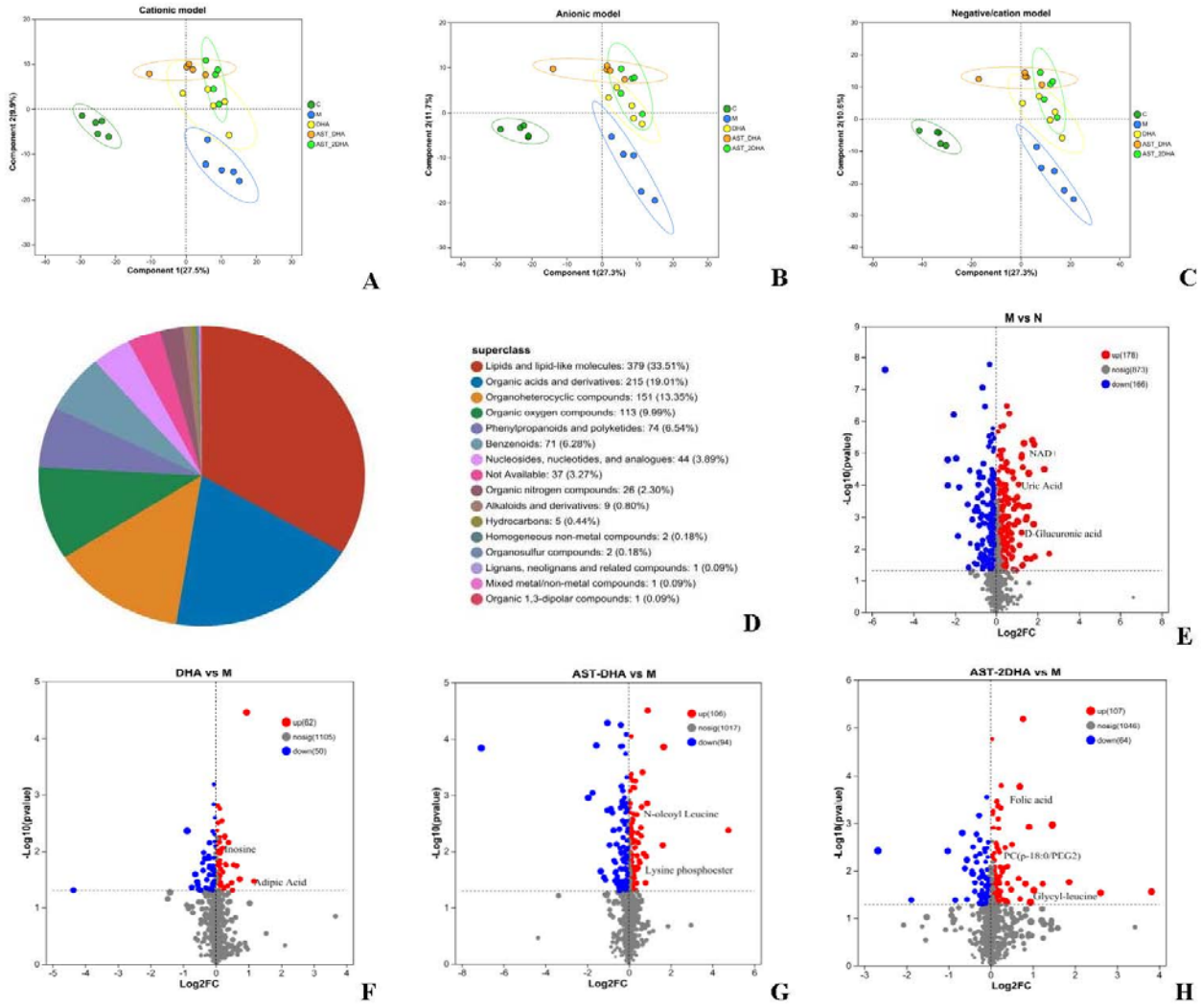

Figure 7. Effects of AST-DHAs on renal metabolism in CP-induced AKI in mice. (A–C) Partial least squares discriminant analysis of mouse renal metabolites. (D) Classification and proportion of differential metabolites in mouse kidneys. (E–H) Volcanic maps of up-regulated and down-regulated renal differential metabolites in the different treatment groups.

3.10 Differentially abundant metabolite analysis

Clustering results revealed that the differentially abundant metabolites in the different treatment groups were grouped into different branches (Figure 8A). The dendrogram of metabolite clustering showed variations in the differentially abundant metabolites found in the kidneys of mice across various treatment groups. In the M group, the metabolites that were notably upregulated primarily consisted of "lipids and lipid-like molecules" as well as "organic acids and their derivatives." In the treatment groups of AST-DHA and AST-2DHA, the metabolites that showed differential abundance primarily encompassed "organic acids along with their derivatives," "lipids and similar lipid-like compounds," and "amino acids." Following this, we conducted a KEGG pathway enrichment analysis for the potential targets. The KEGG analysis indicated that the pathways most notably influenced in the M group relative to the C group were the lipid metabolism and cAMP signaling pathways (Figure 8C). Importantly, iron death is strongly associated with lipid metabolism, and the cAMP signaling pathway can affect cell metabolism, stress response, and cell death. In comparison, the pathways that were most notably impacted in the AST-DHA and AST-2DHA treatment groups, as opposed to the M group, included amino acid metabolism as well as the digestion and absorption

of vitamins (Figure 8E,F). amino acid metabolism is an important component of the ferroptosis mechanism, and its significant expression can inhibit ferroptosis.[32] These findings are consistent with the results of immunofluorescence analysis, which demonstrated that AST-DHAs may modulate related pathways affecting ferroptosis.

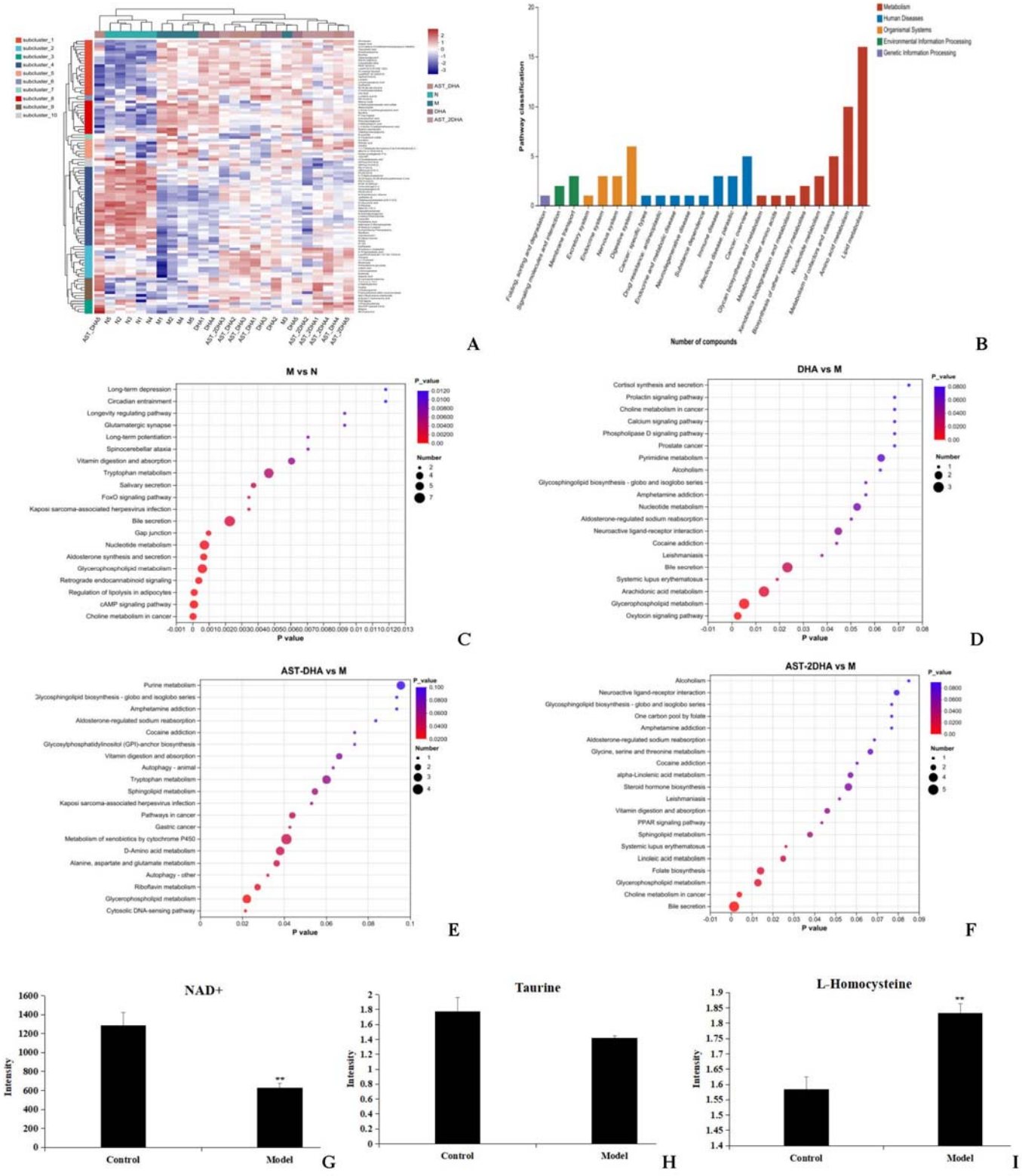

Figure 8. Analysis of the differences in kidney metabolites in mice treated with DHA, AST-DHA and AST-2DHA and the difference of kidney metabolite abundance between group C and group M. (A) Clustering heat maps of differential metabolites under different group treatments, with red and blue indicating the normalized abundance of differential metabolites. (B) Total metabolic pathway analysis. (C–F) The KEGG pathway enrichment bubble diagrams display the significance of enrichment on the horizontal axis represented by the P-value; a smaller P-value indicates greater statistical

significance, while the KEGG pathway is illustrated on the vertical axis. The bubble size indicates the extent of enrichment within the pathway. (G) Variations in NAD+ levels; (H) variations in taurine levels; (I) variations in L-homocysteine levels. The data presented in G–I are shown as mean ± S.E.M. from a study involving 8 mice. ** Indicates a significant difference compared to the normal group ($p < 0.01$). ## Indicates a significant difference compared to the model group ($p < 0.01$).

3.11 Metabolite relative abundance analysis

The above findings revealed that acute kidney injury can be alleviated by inhibiting the iron death pathway, in which amino acid and lipid metabolism are the basis of the iron death mechanism; therefore, we analyzed the abundance of several related metabolites. These studies indicate that AKI can be alleviated by inhibiting the iron death pathway, in which amino acid and lipid metabolism are the basis of the iron death mechanism; therefore, we analyzed the abundance of several related metabolites. Studies have shown that taurine can alleviate iron death-induced damage to myoblast metabolism by reducing unstable iron pools and improving REDOX homeostasis. In addition, taurine inhibits iron death in prostate cancer.[33] In addition, NAD+ depletion leads to downregulation of SLC7A11 and GPX4, resulting in iron death.[34] Studies have shown that when homocysteine is supplemented in the medium, it enhances iron death rather than driving resistance to iron death.[35] As shown in Figure 8G–I, our results revealed that, compared with those in group C, taurine and NAD+ levels in group M were significantly lower ($p < 0.01$) and the homocysteine content was significantly greater ($p < 0.01$). The results revealed that the content of metabolites related to iron death changed significantly in group M, which once again verified that CP-induced AKI is closely related to the pathway of iron death and that AKI can be treated by inhibiting ferroptosis.

4. Discussion

Acute kidney injury (AKI) has become a major public health problem worldwide because of its complex etiology and diverse pathogenesis.[36] In recent years, multiple studies have shown that nutritional intervention is an effective strategy for treating and alleviating kidney disease.[37] In particular, astaxanthin (AST) and docosahexaenoic acid (DHA) have been shown to have significant protective effects against kidney disease.[37] In this context, we synthesized a novel DHA ester compound, astaxanthin-DHA esters (AST-DHAs), and explored its protective properties and potential in a cisplatin (CP)-induced AKI model. mechanism.

To the best of our knowledge, this study is the first to investigate the effect of AST-DHAs on CP-induced AKI. Our results show that AST-DHAs have significant protective effects on AKI mice. Specifically, AST-DHAs significantly reversed edema and congestion in mouse kidneys after CP injection and improved the renal function of the mice, findings that are consistent with those of previous studies.[38] In addition, liver weight and its index also showed similar trends. Observation of renal tissue pathological sections and Masson staining (Figure 2A, B) further confirmed that AST-DHAs significantly improved pathological changes, such as proximal tubule vacuolization, tissue inflammation, renal tubular dilation, and renal fibrosis, in the kidneys of AKI mice. These results indicate that dietary supplementation with DHA-acylated astaxanthin ester has a greater ameliorative effect on CP-induced acute kidney injury than does supplementation with AST or DHA alone. Among the oxidative stress-related indicators, AST-DHAs significantly reduced malondialdehyde (MDA) levels, whereas superoxide dismutase (SOD), glutathione (GSH) and glutathione peroxidase

(GSH-Px) levels significantly increased, and the serum oxidative stress index also showed a similar trend. This result is consistent with the study by Bennedsen et al., who reported that AST-DHAs significantly enhanced the antioxidant capacity of mice, further supporting their potential in the treatment of oxidative stress.[18]

Lipid peroxidation is an important result of oxidative stress. Further peroxidation of its products aggravates the oxidative damage of cells and results in a vicious cycle.[39] Previous studies have shown that increased fatty acid metabolism has protective effects on both acute and chronic kidney injury models.[40] In this study, compared with those in the normal control group (Group C), the levels of saturated fatty acids and unsaturated fatty acids in the AKI model group (Group M) were significantly lower. However, after pretreatment with AST-DHAs, the contents of both fatty acids increased compared with those in the M group, indicating that AST-DHAs can regulate disordered fatty acid metabolism in the kidneys of AKI mice. Notably, AKI caused by multiple factors is closely related to fatty acid metabolism disorders, especially in terms of increased renal free fatty acid levels and significant reductions in long-chain fatty acids (such as palmitic acid and stearic acid).[41] In addition, omega-3 polyunsaturated fatty acids (e.g., DHA) have been shown to slow the progression of chronic kidney disease, which is consistent with our finding that AST-DHAs attenuate decreased levels of palmitic acid, stearic acid, and DHA in the kidneys of AKI mice. consistent.[42] By analyzing small molecule metabolites in biological samples, metabolomics can identify characteristic metabolites related to kidney damage and reveal the metabolic pathways and biological mechanisms involved. Therefore, we used liquid chromatography–mass spectrometry (LC–MS) nontargeted metabolomics technology to study the changes in renal metabolism in AKI mice.[43] Studies have shown that lipid and amino acid metabolism in the kidney is very active under normal circumstances and that the autophagy pathway may play a protective role in sepsis-induced AKI.[44] In this study, the differentially abundant metabolites of group M were enriched mainly in pathways related to lipid metabolism, choline metabolism, amino acid metabolism, riboflavin metabolism, and autophagy. After treatment with AST-DHAs, amino acid metabolism and autophagy were significantly enhanced. Studies have also shown that during amino acid metabolism, tyrosine, tryptophan, aspartic acid and arginine are closely related to ferroptosis.[45] Compared with those in group C, the levels of tyrosine, tryptophan, and aspartic acid in the kidney tissue of the mice in group M were significantly lower, whereas the content of arginine was significantly greater. However, the levels of these amino acids were significantly reversed after AST-DHA treatment, and the abundances of other metabolites also showed similar trends. These results indicate that AST-DHAs may alleviate renal metabolic disorders in AKI mice by inhibiting ferroptosis-related pathways and provide data supporting their use as dietary interventions or therapeutic agents for the treatment of CP-induced AKI.

On the basis of the metabolomic results, we further detected the expression of ferroptosis-related proteins. Glutathione peroxidase 4 (GPX4) is a key enzyme for lipid peroxide degradation and a regulator of ferroptosis.[46] In addition to GPX4, System xCT protects cells from reactive oxygen species (ROS) by promoting the reduction of glutathione (GSH), converting accumulated lipid hydroperoxides in cells into lipid

alcohols and reducing peroxide-related products.[47] induced damage and ferroptosis. Therefore, the GPX4-GSH-System xCT pathway is currently one of the main regulatory pathways for ferroptosis.[48] In this study, AST-DHAs significantly upregulated the expression levels of GPX4 and xCT. In addition, the immunohistochemistry results revealed that AST-DHAs significantly reduced iron accumulation in the kidneys of AKI mice, further confirming that the therapeutic effect of AST-DHAs on AKI was greater than that of AST or DHA alone. Previous studies by our research group also confirmed this: in a 1-methyl-4-phenyl-1,2,3,6-tetrahydropyridine (MPTP)-induced Parkinson's disease animal model, DHA-acylated shrimp cyanine esters are superior to unesterified AST and DHA in relieving symptoms of Parkinson's disease.[17] These results indicate that AST-DHAs inhibit the development of AKI by inhibiting ferroptosis-related pathways and provide strong data support for subsequent research.

In summary, dietary supplementation with AST-DHAs improves CP-induced ferroptosis and oxidative stress to a certain extent and regulates lipid metabolism levels. Its potential mechanism in CP-induced AKI is shown in Figure 9. Furthermore, sample differences had no significant effect on serum uric acid levels, which may be due to the shorter intervention period (12 days). Many studies have shown that the use of nephrotoxic drugs (such as CP) can lead to renal hemodynamic abnormalities, fibrosis, and oxidative stress in mice.[49] Renal hemodynamic abnormalities mainly manifest as glomerular hyperfiltration and hyperperfusion, increased renal blood flow, and an increased glomerular filtration rate.[50] These abnormalities are closely related to elevated serum creatinine (CRE) and uric acid (UA) levels.[51] Therefore, we speculate that supplementation with AST-DHAs may not significantly improve renal hemodynamics or significantly reduce the levels of biomarkers related to renal function. Future research will further explore the specific mechanism of action of AST-DHAs to provide more effective strategies for the treatment of AKI.

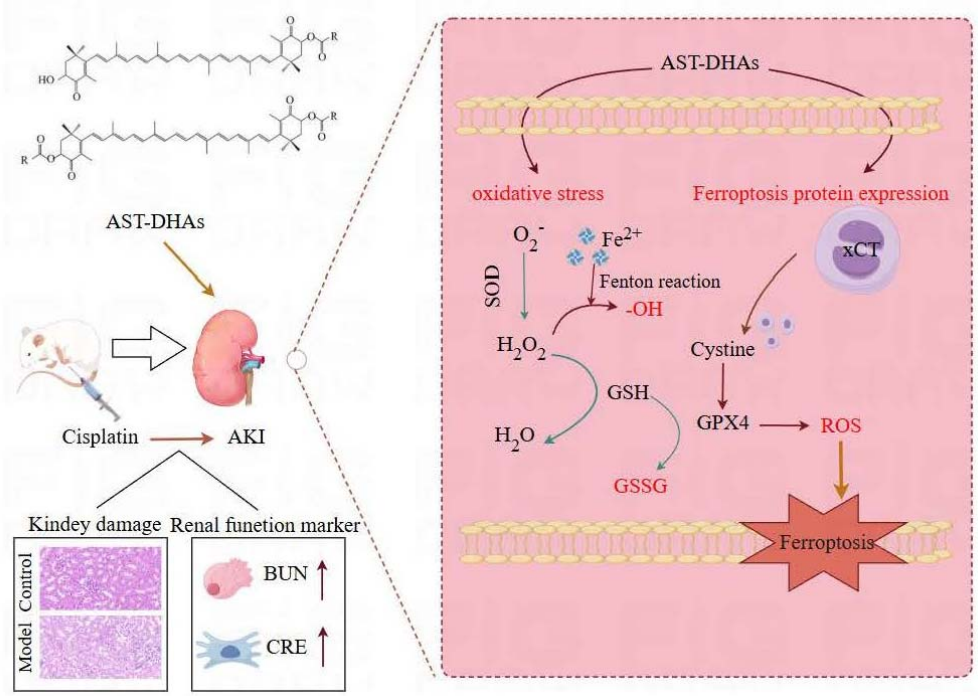

Figure 9. Effect and mechanism of AST-DHAs in cisplatin-induced AKI. In the molecular structures the R groups are DHA.

5. Conclusion

In summary, this research focused on exploring the protective properties of AST-DHAs against CP-induced AKI and the mechanisms involved. The pharmacodynamic findings demonstrated that AST-DHAs effectively improved renal function and reduced pathological damage in mice with AKI. Additionally, it helped to mitigate weight loss and foster renal growth and development. A comparison of AST-DHA and AST-2DHA revealed that the effect of AST-2DHA was generally greater than that of AST-DHA alone. The possible reason is that AST-2DHA contains two fatty acid ester bonds in its molecular structure. Compared with a single ester, this double ester structure can provide better chemical stability, such as putting on a thicker layer of "protective clothing" to the active group, so that it is less prone to oxidative decomposition after storage and entering the body environment, thus ensuring that AST-2DHA can play a more complete active form of treatment. The results showed that AST-DHAs reduced oxidative stress and inhibited ferroptosis by increasing the expression of GPX4 and xCT in a mouse model of AKI. In addition, AST-DHAs can regulate disorders of metabolites and fatty acids in mice with AKI and maintain normal levels in the body. Taken together, these results suggest that AST-DHAs have potential as therapeutic adjuvants for alleviating AKI.

Data availability

The data that support the findings of this study are available from the corresponding author upon reasonable request.

Conflicts of interest

The authors declare that they have no known competing financial interests or personal relationships that could have appeared to influence the work reported in this paper.

Acknowledgements

This work was financially supported by the Key Laboratory of Food Nutrition and Functional Food of Hainan Province (KF202202), by the Project supported by the Education Department of Hainan Province (Hnky2023-3), by the National Natural Science Foundation of China (22308073).

References

(1) Levey, A. S.; Eckardt, K. U.; Dorman, N. M.; Christiansen, S. L.; Hoorn, E. J.; Ingelfinger, J. R.; Inker, L. A.; Levin, A.; Mehrotra, R.; Palevsky, P. M.; et al. Nomenclature for kidney function and disease: report of a Kidney Disease: Improving Global Outcomes (KDIGO) Consensus Conference. *Kidney Int.* **2020**, *97* (6), 1117-1129.

(2) Floege, J.; Mak, R. H.; Molitoris, B. A.; Remuzzi, G.; Ronco, P. Nephrology research--the past, present and future. *Nat Rev Nephrol* **2015**, *11* (11), 677-687.

(3) Allison, S. J. Propagation of acute kidney injury. *Nat Rev Nephrol* **2023**, *19* (10), 622.

(4) Turgut, F.; Awad, A. S.; Abdel-Rahman, E. M. Acute Kidney Injury: Medical Causes and Pathogenesis. *J Clin Med* **2023**, *12* (1).

(5) Li, J. C.; Wang, L. J.; Feng, F.; Chen, T. T.; Shi, W. G.; Liu, L. P. Role of heparanase in sepsis-related acute kidney injury (Review). *Exp Ther Med* **2023**, *26* (2), 379.

(6) Han, C.; Sun, T.; Liu, Y.; Fan, G.; Zhang, W.; Liu, C. Protective effect of Polygonatum sibiricum polysaccharides on gentamicin-induced acute kidney injury in rats via inhibiting p38 MAPK/ATF2 pathway. *Int. J. Biol. Macromol.* **2020**, *151*, 595-601.

(7) Meng, H.; Fu, G.; Shen, J.; Shen, K.; Xu, Z.; Wang, Y.; Jin, B.; Pan, H. Ameliorative Effect of Daidzein on Cisplatin-Induced Nephrotoxicity in Mice via Modulation of Inflammation, Oxidative Stress, and Cell Death. *Oxid. Med. Cell. Longev.* **2017**, *2017*, 3140680.

(8) Di Mascio, P.; Devasagayam, T. P.; Kaiser, S.; Sies, H. Carotenoids, tocopherols and thiols as biological singlet molecular oxygen quenchers. *Biochem. Soc. Trans.* **1990**, *18* (6), 1054-1056.
(9) Etoh, H.; Suhara, M.; Tokuyama, S.; Kato, H.; Nakahigashi, R.; Maejima, Y.; Ishikura, M.; Terada, Y.; Maoka, T. Auto-oxidation products of astaxanthin. *J. Oleo Sci.* **2012**, *61* (1), 17-21.
(10) Qiao, X.; Yang, L.; Hu, X.; Cao, Y.; Xue, C. Characterization and evaluation of inclusion complexes between astaxanthin esters with different molecular structures and hydroxypropyl-β-cyclodextrin. *Food Hydrocolloids* **2020**, 106208.
(11) Chen, Y. Y.; Lee, P. C.; Wu, Y. L.; Liu, L. Y. In Vivo Effects of Free Form Astaxanthin Powder on Anti-Oxidation and Lipid Metabolism with High-Cholesterol Diet. *PLoS ONE* **2015**, *10* (8), e0134733.
(12) Kobayashi, M.; Sakamoto, Y. Singlet oxygen quenching ability of astaxanthin esters from the green alga Haematococcus pluvialis. *Biotechnol. Lett.* **1999**, *21* (4), 265-269.
(13) Rao, A. R.; Sindhuja, H. N.; Dharmesh, S. M.; Sankar, K. U.; Sarada, R.; Ravishankar, G. A. Effective Inhibition of Skin Cancer, Tyrosinase, and Antioxidative Properties by Astaxanthin and Astaxanthin Esters from the Green Alga *Haematococcus pluvialis*. *J. Agric. Food Chem.* **2013**, *61* (16), 3842-3851.
(14) Kamath, B. S.; Srikanta, B. M.; Dharmesh, S. M.; Sarada, R.; Ravishankar, G. A. Ulcer preventive and antioxidative properties of astaxanthin from Haematococcus pluvialis. *Eur. J. Pharmacol.* **2008**, *590* (1-3), 387-395.
(15) jr, A. A. K.; Kagan, V. E.; Minin, A. A. Quenching of singlet oxygen luminescence by fatty acids and lipids: Contribution of physical and chemical mechanisms. *FEBS Lett.* **1983**.
(16) Hussein, G.; Sankawa, U.; Goto, H.; Matsumoto, K.; Watanabe, H. Astaxanthin, a carotenoid with potential in human health and nutrition. *J. Nat. Prod.* **2006**, *69* (3), 443-449.
(17) Wang, C. C.; Shi, H. H.; Xu, J.; Yanagita, T.; Xue, C. H.; Zhang, T. T.; Wang, Y. M. Docosahexaenoic acid-acylated astaxanthin ester exhibits superior performance over non-esterified astaxanthin in preventing behavioral deficits coupled with apoptosis in MPTP-induced mice with Parkinson's disease. *Food Funct* **2020**, *11* (9), 8038-8050.
(18) Bennedsen, M.; Wang, X.; Willén, R.; Wadström, T.; Andersen, L. P. Treatment of H. pylori infected mice with antioxidant astaxanthin reduces gastric inflammation, bacterial load and modulates cytokine release by splenocytes. *Immunol. Lett.* **1999**, *70* (3), 185-189.
(19) Lee, D. H.; Kim, C. S.; Lee, Y. J. Astaxanthin protects against MPTP/MPP+-induced mitochondrial dysfunction and ROS production in vivo and in vitro. *Food Chem. Toxicol.* **2011**, *49* (1), 271-280.
(20) Yang, L.; Qiao, X.; Liu, J.; Wu, L.; Cao, Y.; Xu, J.; Xue, C. Preparation, characterization and antioxidant activity of astaxanthin esters with different molecular structures. *J. Sci. Food Agric.* **2021**, *101* (6), 2576-2583.
(21) Ali, B. H.; Abdelrahman, A.; Al Suleimani, Y.; Manoj, P.; Ali, H.; Nemmar, A.; Al Za'abi, M. Effect of concomitant treatment of curcumin and melatonin on cisplatin-induced nephrotoxicity in rats. *Biomed Pharmacother* **2020**, *131*, 110761.
(22) Zhang, H.; He, Y.; Song, C.; Chai, Z.; Liu, C.; Sun, S.; Huang, Q.; He, C.; Zhang, X.; Zhou, Y.; Zhao, F. Analysis of fatty acid composition and sensitivity to dietary n-3 PUFA intervention of mouse n-3 PUFA-enriched tissues/organs. *Prostaglandins Leukot. Essent. Fatty Acids* **2023**, *192*, 102568.
(23) Song, Y.; Wang, B.; Zhu, X.; Hu, J.; Sun, J.; Xuan, J.; Ge, Z. Human umbilical cord blood-derived MSCs exosome attenuate myocardial injury by inhibiting ferroptosis in acute myocardial infarction mice. *Cell Biol. Toxicol.* **2021**, *37* (1), 51-64.
(24) Zheng, C.; Huang, L.; Luo, W.; Yu, W.; Hu, X.; Guan, X.; Cai, Y.; Zou, C.; Yin, H.; Xu, Z.; et al. Inhibition of STAT3 in tubular epithelial cells prevents kidney fibrosis and nephropathy in STZ-induced diabetic mice. *Cell Death Dis.* **2019**, *10* (11), 848.
(25) Cheng, Q.; Zhang, J.; Fang, J.; Ding, H.; Xu, Y.; Lu, X.; Zhang, W. Untargeted metabolomics reveals the role of AQP9 in nonalcoholic fatty liver disease in a mice model. *Int. J. Biol. Macromol.* **2022**, *219*, 864-875.
(26) Banerjee, R.; Bultman, S. J.; Holley, D.; Hillhouse, C.; Bain, J. R.; Newgard, C. B.; Muehlbauer, M. J.; Willis, M. S. Non-targeted metabolomics of Brg1/Brm double-mutant cardiomyocytes reveals a novel role for SWI/SNF complexes in metabolic homeostasis. *Metabolomics* **2015**, *11* (5), 1287-1301.
(27) Hu, T.; Yue, J.; Tang, Q.; Cheng, K. W.; Chen, F.; Peng, M.; Zhou, Q.; Wang, M. The effect of quercetin on diabetic nephropathy (DN): a systematic review and meta-analysis of animal studies. *Food Funct* **2022**, *13* (9), 4789-4803.
(28) Brown, K.; Comisar, C.; Witjes, H.; Maringwa, J.; de Greef, R.; Vishwanathan, K.; Cantarini, M.; Cox, E. Population pharmacokinetics and exposure-response of osimertinib in patients with non-small cell lung cancer. *Br. J. Clin. Pharmacol.* **2017**, *83* (6), 1216-1226.
(29) Mohamadi Yarijani, Z.; Najafi, H. Kidney injury in COVID-19 patients, drug development and their renal complications: Review study. *Biomed Pharmacother* **2021**, *142*, 111966.
(30) Mao, L.; Wang, X.; Sun, Y.; Yang, M.; Chen, X.; Cui, L.; Bai, W. Platelet-rich fibrin improves repair and regeneration of damaged endometrium in rats. *Front Endocrinol (Lausanne)* **2023**, *14*, 1154958.
(31) Naughton, S. S.; Mathai, M. L.; Hryciw, D. H.; McAinch, A. J. Linoleic acid and the pathogenesis of obesity. *Prostaglandins Other Lipid Mediat* **2016**, *125*, 90-99.
(32) Yang, Z.; Zou, S.; Zhang, Y.; Zhang, J.; Zhang, P.; Xiao, L.; Xie, Y.; Meng, M.; Feng, J.; Kang, L.; et al. ACTL6A protects gastric cancer cells against ferroptosis through induction of glutathione synthesis. *Nat. Commun.* **2023**, *14* (1), 4193.
(33) Xiao, H.; Du, X.; Tao, Z.; Jing, N.; Bao, S.; Gao, W. Q.; Dong, B.; Fang, Y. X. Taurine Inhibits Ferroptosis Mediated by the Crosstalk between Tumor Cells and Tumor-Associated Macrophages in Prostate Cancer. *Adv Sci (Weinh)* **2024**, *11* (3), e2303894.
(34) Chen, X.; Wang, Z.; Li, C.; Zhang, Z.; Lu, S.; Wang, X.; Liang, Q.; Zhu, X.; Pan, C.; Wang, Q.; et al. SIRT1 activated by AROS sensitizes glioma cells to ferroptosis via induction of NAD+ depletion-dependent activation of ATF3. *Redox Biol* **2024**, *69*, 103030.
(35) Jiang, X.; Stockwell, B. R.; Conrad, M. Ferroptosis: mechanisms, biology and role in disease. *Nat Rev Mol Cell Biol* **2021**, *22*

(4), 266-282.
(36) Mehta, R. L.; Kellum, J. A.; Shah, S. V.; Molitoris, B. A.; Ronco, C.; Warnock, D. G.; Levin, A. Acute Kidney Injury Network: report of an initiative to improve outcomes in acute kidney injury. *Crit. Care* **2007**, *11* (2), 31.
(37) Khajavi Rad, A.; Mohebbati, R.; Hosseinian, S. Drug-induced Nephrotoxicity and Medicinal Plants. *Iran J Kidney Dis* **2017**, *11* (3), 169-179.
(38) Lebwohl, D.; Canetta, R. Clinical development of platinum complexes in cancer therapy: an historical perspective and an update. *Eur. J. Cancer* **1998**, *34* (10), 1522-1534.
(39) Mortensen, M. S.; Ruiz, J.; Watts, J. L. Polyunsaturated Fatty Acids Drive Lipid Peroxidation during Ferroptosis. *Cells* **2023**, *12* (5).
(40) Sun, T.; Wang, D.; Wang, B.; Liu, X.; Li, N.; Shi, K. Melatonin attenuates cisplatin-induced acute kidney injury in mice: Involvement of PPARα and fatty acid oxidation. *Food Chem. Toxicol.* **2022**, *163*, 112970.
(41) Liu, B.; Jie, X.; Deng, J.; Zhang, S.; Lu, F.; Liu, X.; Zhang, D. Bupi Yishen formula may prevent kidney fibrosis by modulating fatty acid metabolism in renal tubules. *Phytomedicine* **2023**, *114*, 154767.
(42) Gai, Z.; Wang, T.; Visentin, M.; Kullak-Ublick, G. A.; Fu, X.; Wang, Z. Lipid Accumulation and Chronic Kidney Disease. *Nutrients* **2019**, *11* (4).
(43) Wen, Y., Parikh, C. R. Current concepts and advances in biomarkers of acute kidney injury. *Critical reviews in clinical laboratory sciences* **2021,** 58(5), 354-368.
(44) Garibotto, G.; Sofia, A.; Saffioti, S.; Bonanni, A.; Mannucci, I.; Verzola, D. Amino acid and protein metabolism in the human kidney and in patients with chronic kidney disease. *Clin. Nutr.* **2010**, *29* (4), 424-433.
(45) Btaiche, I. F.; Mohammad, R. A.; Alaniz, C.; Mueller, B. A. Amino Acid Requirements in Critically Ill Patients with Acute Kidney Injury Treated with Continuous Renal Replacement Therapy. *Pharmacotherapy: The Journal of Human Pharmacology and Drug Therapy* **2008**, *28*.
(46) Verstockt, S.; Machiels, K.; Dehairs, J.; Rems, K.; Jans, D.; Greef, I. D.; Sabino, J.; Ferrante, M.; Verstockt, B.; Vermeire, S. Sa1809 Gene Networks In Post-Operative Endoscopic Recurrence In Crohn's Disease: A Key Role For Ferroptosis Gene GPX4. *Gastroenterology* **2023**.
(47) Maiorino, M.; Conrad, M.; Ursini, F. GPx4, Lipid Peroxidation, and Cell Death: Discoveries, Rediscoveries, and Open Issues. *Antioxid Redox Signal* **2018**, *29* (1), 61-74.
(48) Wang, X.; Lin, Z.; Li, T.; Zhu, W.; Huang, H.; Hu, J.; Zhou, J. Sodium Selenite Prevents Matrine-Induced Nephrotoxicity by Suppressing Ferroptosis via the GSH-GPX4 Antioxidant System. *Biological trace element research.* **2024**, (10), 202.
(49) Mody, H.; Ramakrishnan, V.; Chaar, M.; Lezeau, J.; Rump, A.; Taha, K.; Lesko, L.; Ait-Oudhia, S. A Review on Drug-Induced Nephrotoxicity: Pathophysiological Mechanisms, Drug Classes, Clinical Management, and Recent Advances in Mathematical Modeling and Simulation Approaches. *Clin Pharmacol Drug Dev* **2020**, *9* (8), 896-909.
(50) Matejovic, M.; Ince, C.; Chawla, L. S.; Blantz, R.; Molitoris, B. A.; Rosner, M. H.; Okusa, M. D.; Kellum, J. A.; Ronco, C. Renal Hemodynamics in AKI: In Search of New Treatment Targets. *J. Am. Soc. Nephrol.* **2016**, *27* (1), 49-58.
(51) Lin, P.; Wu, M.; Qin, J.; Yang, J.; Ye, C.; Wang, C. Magnesium lithospermate B improves renal hemodynamics and reduces renal oxygen consumption in 5/6th renal ablation/infarction rats. *BMC Nephrol.* **2019**, *20* (1), 49.